Ji et al. PhotoniX (2024) 5:13
https://doi.org/10.1186/s43074-024-00125-8

PhotoniX

RESEARCH Open Access

High-dimensional Poincaré beams generated through cascaded metasurfaces for high-security optical encryption

Jitao Ji[1], Chen Chen[1*], Jiacheng Sun[1], Xin Ye[1], Zhizhang Wang[1], Jian Li[1], Junyi Wang[1], Wange Song[1], Chunyu Huang[1], Kai Qiu[1], Shining Zhu[1] and Tao Li[1*]

*Correspondence: chenchen2021@nju.edu.cn; taoli@nju.edu.cn

[1] National Laboratory of Solid State Microstructures, Key Laboratory of Intelligent Optical Sensing and Manipulation, Jiangsu Key Laboratory of Artificial Functional Materials, College of Engineering and Applied Sciences, Nanjing University, Nanjing 210093, China

Abstract

Optical encryption plays an increasingly important role in the field of information security owing to its parallel processing capability and low power consumption. Employing the ultrathin metasurfaces in optical encryption has promoted the miniaturization and multifunctionality of encryption systems. Nevertheless, with the few number of degrees of freedom (DoFs) multiplexed by single metasurface, both key space and encoding space are limited. To address this issue, we propose a high-security and large-capacity optical encryption scheme based on perfect high-dimensional Poincaré beams with expanded DoFs. By cascading two arrayed metasurfaces, more beam properties can be independently engineered, which gives rise to the extensively expanded key and encoding spaces. Our work provides a promising strategy for optical encryption with high security level and large information capacity and might facilitate the applications of Poincaré beams in optical communications and quantum information.

Keywords: Poincaré beams, Cascaded metasurfaces, Optical encryption

Introduction

With the rapid development of information technology, information security is becoming of vital significance and so do the derived encryption techniques. Optical encryption possesses the advantages of parallel processing, large capacity and low power consumption, and offers an ideal platform for information protection owing to abundant degrees of freedom (DoFs) of the photon [1–5]. However, conventional optical encryption system commonly involves in a series of complicated optical elements and results in a bulky volume. In addition, due to the limited optical field manipulation capability of traditional optical elements, the multi-dimensional DoFs of light have not been fully exploited.

As an ultra-thin planar optical element composed of subwavelength nanostructures, metasurface has shown powerful capability of multi-dimensional optical field manipulation and emerges as a promising candidate for optical encryption in a compact form [6–13]. For metasurface-empowered optical encryption system, the key space could be defined as the total number of keys and attributed to both incident and output states.

While the encoding space refers to the information capacity of the output images or beams through metasurfaces. So far, various DoFs of light, including incident angle [14–16], wavelength [17], polarization [18, 19], orbital angular momentum (OAM) mode [20–23] and so on [24, 25], have been explored to construct key space for optical information security. The combination of multiple DoFs has been demonstrated the capability to enhance the complexity of keys [26–30]. Besides, through encoding information into optical images in the form of nano-printing or holography, encoding space has also been established and depends on the number of multiplexing channels of metasurface [31, 32]. To further expand the key and encoding spaces, encryption algorithms and dynamic encryption schemes were aroused for high security and large capacity performance [33–38]. Nevertheless, the above two strategies usually suffer from time-consuming decryption process and the lack of pixelated real-time modulation. Featured with spatial variant polarization states and phase distributions, Poincaré beams gain a great deal of attentions in many applications [39–44], especially in optical encryption and encoding owing to versatile independent DoFs [45–49]. In the recent works, optical information was encoded into the polarization order and ellipticity of perfect hybrid-order Poincaré beams (HyOPBs) [45]. It presents a new scheme of optical encryption to enlarge the encoding space, which is distinguished from conventional nanoprinting or holography encryption. However, such Poincaré beams encryption strategy has constraints due to limited key space (with only one incident state in essence) and stays a low security level. With the advantages of sub-wavelength modulation capability and inherent ultra-thin size, metasurface also allows spatial multiplexing frameworks such as arrayed metasurface [45] and cascaded metasurfaces [25, 50–52]. Therefore, the combination of cascaded and arrayed metasurfaces boasts great potentials for enhancement of key and encoding spaces towards high-security and large-capacity features.

In this work, we propose a high-security and large-capacity optical encryption strategy based on multi-channel perfect high-dimensional Poincaré beams (HDPBs) generated by cascaded metasurfaces. Benefiting from the infinite modes of HDPBs and the scalability of arrayed metasurface, both key space and encoding space have been considerably expanded. Accordingly, by cascading two arrayed metasurfaces composed of 16×10 cells, an optical encryption platform is implemented by encoding information into five independent parameters of HDPBs. Our work provides a promising solution to extensively enlarge the key and encoding spaces and may open an avenue towards advanced optical encryption systems.

Results

Concept and principle of high-dimensional Poincaré beams encryption

Figure 1 schematically illustrates the HDPBs optical encryption scheme using cascaded metasurfaces, which is capable of generating multi-channel HDPBs with diverse DoFs to encode optical information. In principle, HyOPBs can be described as a linear superposition of right-handed circular polarized (RCP) and left-handed circular polarized (LCP) bases with different topological charges [39]. Here, we generalize a more complex vector vortex beam superposed by two HyOPBs as HDPBs, which can be represented by high-dimensional Poincaré sphere indicated by the magenta or blue sphere in Fig. 1. Taking the blue sphere for instance, the north

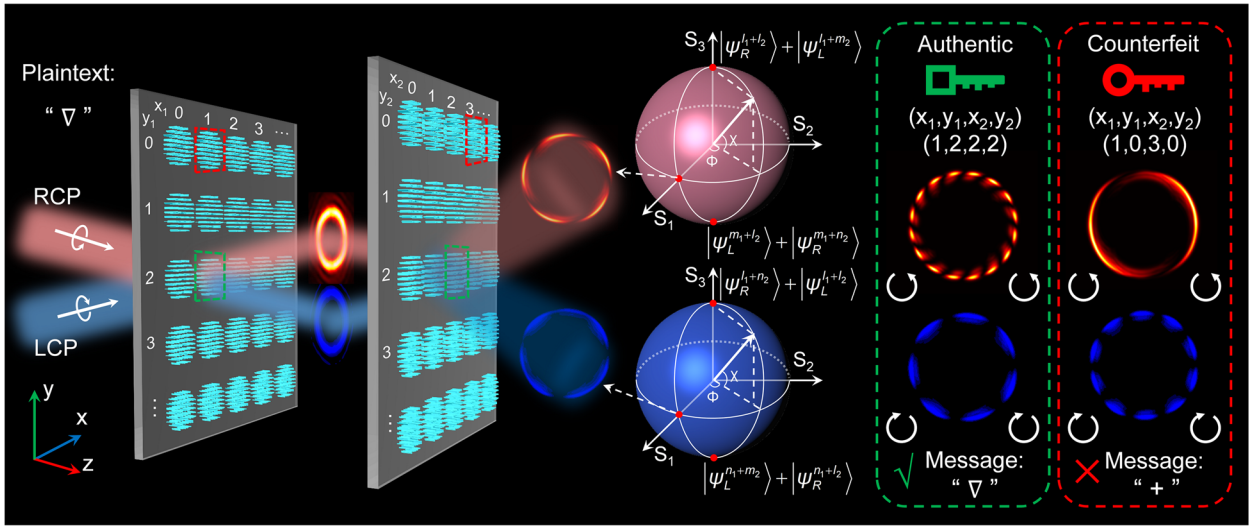

Fig. 1 Schematic illustration of cascaded metasurfaces based perfect HDPBs for optical encryption. The plaintext is encrypted into two cascaded metasurfaces with multiple cells. According to the customized keys in the form of coordinates (x_1, y_1, x_2, y_2) of two arrayed metasurfaces, cascading two specific cells (marked by red dashed lines) could generate two perfect HDPBs under RCP and LCP incidences. The states of two generated HDPBs can be independently described by the magenta and blue high-dimensional Poincaré spheres. Through characterizing the HDPBs by RCP/LCP analyzers for RCP/LCP incidences, the annular intensity distributions (outlined within green/red dashed lines) are presented and could be translated into different messages for information decryption

(south) pole is a linear superposition of RCP and LCP optical vortices with topological charges of l_1+n_2 (n_1+l_2) and l_1+l_2 (n_1+m_2), namely $\left|\psi_R^{l_1+n_2}\right\rangle+\left|\psi_L^{l_1+l_2}\right\rangle$ $(\left|\psi_L^{n_1+m_2}\right\rangle+\left|\psi_R^{n_1+l_2}\right\rangle)$. Arbitrary state $|\psi\rangle$ on the surface of high-dimensional Poincaré sphere can take the form as follows

$$|\psi\rangle=\sin(\frac{\chi}{2}+\frac{\pi}{4})(\left|\psi_R^{l_1+n_2}\right\rangle+\left|\psi_L^{l_1+l_2}\right\rangle)+\cos(\frac{\chi}{2}+\frac{\pi}{4})(\left|{}^{\Phi}\psi_L^{n_1+m_2}\right\rangle+\left|{}^{\Phi}\psi_R^{n_1+l_2}\right\rangle), \tag{1a}$$

where

$$\left|\psi_R^{l_1+n_2}\right\rangle=e^{i(l_1+n_2)\phi}(\hat{e}_x-i\hat{e}_y), \tag{1b}$$

$$\left|\psi_L^{l_1+l_2}\right\rangle=e^{i(l_1+l_2)\phi}(\hat{e}_x+i\hat{e}_y), \tag{1c}$$

$$\left|{}^{\Phi}\psi_L^{n_1+m_2}\right\rangle=e^{i\Phi}e^{i(n_1+m_2)\phi}(\hat{e}_x+i\hat{e}_y), \tag{1d}$$

$$\left|{}^{\Phi}\psi_R^{n_1+l_2}\right\rangle=e^{i\Phi}e^{i(n_1+l_2)\phi}(\hat{e}_x-i\hat{e}_y). \tag{1e}$$

Here, $\sin(\frac{\chi}{2}+\frac{\pi}{4})$ and $\cos(\frac{\chi}{2}+\frac{\pi}{4})$ denote the relative amplitude while Φ is the phase difference of two poles. Also, l_1, m_1, n_1, l_2, m_2 and n_2 are the topological charges and the corresponding numbers 1 and 2 refer to the contributions by two cascaded metasurfaces. R and L are abbreviations of RCP and LCP states. $\hat{e}_x$ and $\hat{e}_y$ represent the unit vectors along x and y axis and ϕ is the azimuth coordinate. For instance, $\left|{}^{\Phi}\psi_L^{n_1+m_2}\right\rangle$ corresponds to the LCP state carried with topological charge of n_1+m_2 and phase of Φ. To acquire such HDPBs, two metasurfaces made up of planar chiral meta-atoms are required to be aligned to generate incident HyOPBs and perfect HDPBs. With the spin-decoupled modulation channels, the generated perfect HDPBs can lie on two different high-dimensional Poincaré spheres (that is the magenta and blue ones) according to the circular polarization states of incident light. In order to encrypt information with higher security and larger capacity, two arrayed metasurfaces are established so as to generate a variety of perfect HDPBs. Once the authentic coordinates (x_1, y_1, x_2, y_2) of two arrayed metasurfaces are obtained, the desired states of HDPBs could be achieved through alignment of two specific metasurfaces. The plaintext can be subsequently decoded by characterizing the properties of HDPBs based on the annular intensity distributions through RCP/LCP analyzers for RCP/LCP incidences. Otherwise, the misalignment of coordinates (a counterfeit key) would lead to generation of wrong HDPBs and make the plaintext unavailable. It should be mentioned that the scale of the arrayed metasurfaces, could be extremely expanded and contributes to a high security level. In addition, the encoding space with dependence on the states of HDPBs can also be enlarged through plenty of combinations of two cascaded metasurfaces.

Generation of multi-channel perfect hybrid-order Poincaré beams

As a precondition for HDPBs encryption, generation of multi-channel perfect HyOPBs should be realized at the first stage. To this end, a single-layer metasurface based on planar chiral meta-atoms is employed for spin-decoupled phase manipulation through breaking the mirror symmetry and higher-order rotational symmetry [53, 54]. As depicted in Fig. 2(a), the transmitted co-polarized ϕ_{co} and two cross-polarized channels ϕ_{RL} and ϕ_{LR} enable three independent phase modulation channels under RCP and LCP incidences (Supplementary Note 1). By incorporating chiral meta-atoms with geometric phase, the designed metasurface can function as a combination of four optical elements, namely a quarter-wave plate, a spiral phase plate, an axicon and a Fourier lens, for generation of multi-channel perfect vortex beams with controllable topological charges of l_0, m_0 and n_0 (see Supplementary Note 2 for detailed phase distributions of chiral meta-atoms). Therefore, through coherent superposition of the co-polarized and cross-polarized perfect vortex beams, two different perfect HyOPBs $(\left|\psi_L^{m_0}\right\rangle + \left|\psi_R^{l_0}\right\rangle$ and $\left|\psi_R^{n_0}\right\rangle + \left|\psi_L^{l_0}\right\rangle)$ can be accessed according to the incident circular polarization states (Supplementary Note 3).

For experimental demonstration, a metasurface made of silicon nitride chiral meta-atoms with height of 1.2 μm on fused silica substrate was prepared (See Methods for fabrication process). Figure 2(b) shows the optical microscope image of the fabricated metasurface with radius of 50 μm and topological charges l_0, m_0 and n_0 of -3, 4 and 1, respectively. Through illuminating 470 nm light, the transmitted beams through metasurface were collected as exhibited in Fig. 2(c) (optical characterization can be referred to

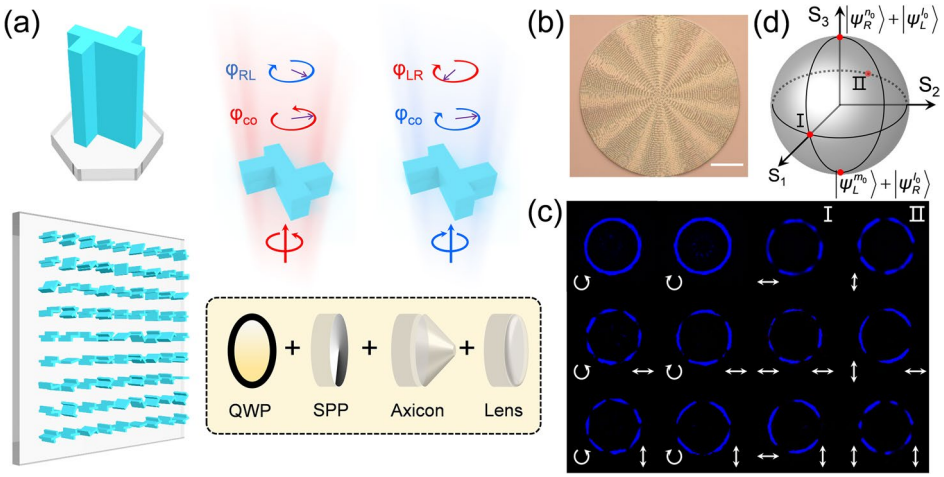

Fig. 2 Generation of multi-channel perfect HyOPBs. **a** Planar chiral meta-atom for phase modulation of co-polarized and cross-polarized channels (φ_{co}, φ_{RL} and φ_{LR}) under RCP and LCP incidences. The single-layer chiral metasurface functions as the combination of quarter-wave plate (QWP), spiral phase plate (SPP), Axcion and Fourier lens. **b** The optical microscope image of the fabricated chiral metasurface. Scale bar: 20 μm. **c** The measured intensity profiles of perfect HyOPBs and HDPBs with topological charges l_0, m_0 and n_0 of -3, 4 and 1 at 470 nm under RCP, LCP, H- and V-polarized incidences. The white arrow in the left corner of each image corresponds to the input polarization state while that in the right corner depicts the polarization state of analyzers. The first row represents the output intensity without polarization analyzers. **d** The high-dimensional Poincaré sphere that describes the states of the generated Poincaré beams under linearly polarized incidences

Methods). The first to fourth columns list the generated beams under RCP, LCP, horizontal linearly polarized (H-polarized) and vertical linearly polarized (V-polarized) incidences. It is clear that the intensities of the generated beams are split into seven and four bright lobes after passing through linear polarization analyzer under RCP and LCP incidences, which correspond to the polarization orders of $\left|\psi_L^4\right\rangle + \left|\psi_R^{-3}\right\rangle$ and $\left|\psi_R^1\right\rangle + \left|\psi_L^{-3}\right\rangle$. Meanwhile, the annular intensity distributions present almost identical radiuses regardless of the number of topological charges. The above experimental results are coincident with the theoretically calculated ones listed in Fig. S2(b), validating the generation of multi-channel perfect HyOPBs. Additionally, these two HyOPBs can be further linearly superposed into HDPBs under linear-polarized incidences, as shown in the third and fourth column in Fig. 2(c). By changing the incident states from H-polarization to V-polarization, the generated perfect HDPBs evolves from point I to II on the equator of high-dimensional Poincaré sphere displayed in Fig. 2(d). Characterized by non-uniformly distributed polarization states with space-variant phase distribution, HDPBs can serve as information carriers to establish an enormous key and encoding spaces for optical encryption.

Manipulation of perfect high-dimensional Poincaré beams

By virtue of the multi-channel phase modulation of planar chiral metasurface, generation of HDPBs has been demonstrated above. Nonetheless, the states of HDPBs are limited within a single metasurface because of the identical co-polarized phase modulation channels. In terms of HDPBs encryption, to achieve larger key and encoding spaces, another metasurface (meta_1) is adopted to generate multi-channel HyOPBs as incidences for the following metasurface (meta_2) (see Supplementary Note 4 for detailed phase modulation design). As illustrated in Fig. 3(a), the incident RCP and LCP light are transformed into two HyOPBs $\left|\psi_R^{l_1}\right\rangle + \left|^{\Phi_{11}}\psi_L^{m_1}\right\rangle$ and $\left|\psi_L^{l_1}\right\rangle + \left|^{\Phi_{12}}\psi_R^{n_1}\right\rangle$ through meta_1. Cascaded by meta_2, the HyOPBs are subsequently modulated into multi-channel perfect HDPBs. In this work, HDPBs are designed to lie on the equator of two high-dimensional Poincaré spheres and can be expressed as (referred to equations S9a-b)

$$|\psi_R\rangle = \left|\psi_R^{l_1+l_2}\right\rangle + \left|^{\Phi_{21}}\psi_L^{l_1+m_2}\right\rangle + \left|^{\Phi_{11}}\psi_L^{m_1+l_2}\right\rangle + \left|^{\Phi_{11}+\Phi_{22}}\psi_R^{m_1+n_2}\right\rangle \tag{2}$$

and

$$|\psi_L\rangle = \left|\psi_L^{l_1+l_2}\right\rangle + \left|^{\Phi_{22}}\psi_R^{l_1+n_2}\right\rangle + \left|^{\Phi_{12}}\psi_R^{n_1+l_2}\right\rangle + \left|^{\Phi_{12}+\Phi_{21}}\psi_L^{n_1+m_2}\right\rangle \tag{3}$$

for RCP and LCP incidences. Φ_{12} and Φ_{11} (Φ_{22} and Φ_{21}) denote the phase differences between co-polarized and cross-polarized channels of meta_1 (meta_2), respectively. After passing through RCP/LCP analyzers, the output beams turn into $\left|\psi_R^{l_1+l_2}\right\rangle + \left|^{\Phi_{11}+\Phi_{22}}\psi_R^{m_1+n_2}\right\rangle$ and $\left|\psi_L^{l_1+l_2}\right\rangle + \left|^{\Phi_{12}+\Phi_{21}}\psi_L^{n_1+m_2}\right\rangle$ for RCP and LCP incidences and appear as annularly distributed bright lobes. Hence, polarization orders of two HDPBs, defined as $P_R=(l_1+l_2\text{-}m_1\text{-}n_2)/2$ and $P_L=(l_1+l_2\text{-}n_1\text{-}m_2)/2$, can be flexibly manipulated by designing six topological charges and emerged as the number of bright lobes. Figure 3(b) and (c) display the top and side view of the scanning electron

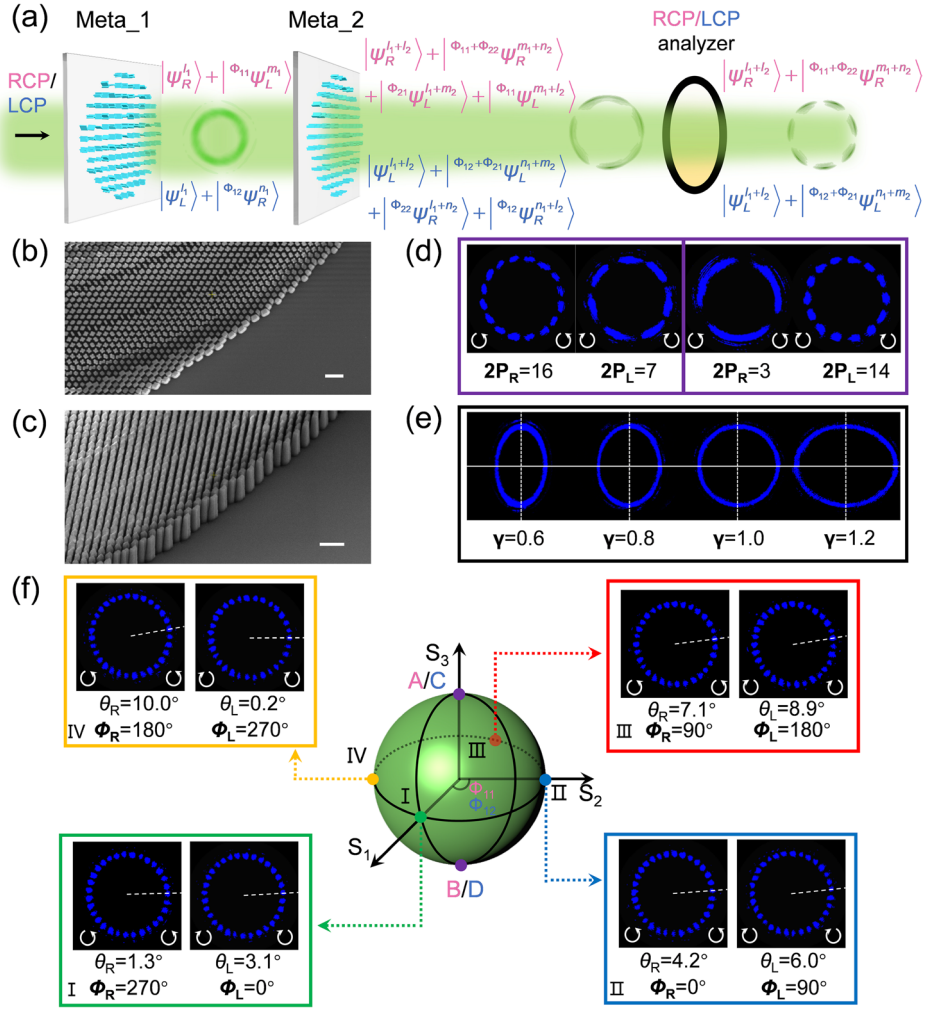

Fig. 3 Manipulation five parameters (P_R, P_L, γ, Φ_R and Φ_L) of HDPBs. **a** Conceptual illustration of generating multi-channel perfect HDPBs via cascaded chiral metasurfaces (meta_1 and meta_2). The generated HDPBs are analyzed by RCP/LCP analyzers for RCP/LCP incidences. **b** Top- and (**c**) side-view scanning electron microscope images of the fabricated metasurface. Scale bars: 1 μm. **d** The intensity distributions of HDPBs under RCP/LCP incidences and analyzers with topological charges of $l_1=7$, $m_1=-5$, $n_1=7$, $l_2=8$, $m_2=1$, $n_2=4$ (left) and $l_1=7$, $m_1=4$, $n_1=-5$, $l_2=8$, $m_2=6$, $n_2=8$ (right) corresponding to polarization orders P_R of 8 and 3/2, P_L of 7/2 and 7. **e** The measured intensity profiles of perfect HDPBs with different ellipticities γ of 0.6, 0.8, 1.0 and 1.2. **f** The generated eight states on the equators of two high-dimensional Poincaré spheres marked by Greek numerals I, II, III and IV. The north and south poles of two high-dimensional Poincaré spheres are indicated by A (C) and B (D) where A (C) represents the state $\left|\psi_R^{l_1+l_2}\right\rangle+\left|\Phi_{21}\psi_L^{l_1+m_2}\right\rangle$ ($\left|\psi_L^{l_1+l_2}\right\rangle+\left|\Phi_{22}\psi_R^{l_1+n_2}\right\rangle$) while B (D) represents the state $\left|\psi_L^{m_1+l_2}\right\rangle+\left|\Phi_{22}\psi_R^{m_1+n_2}\right\rangle$ ($\left|\psi_R^{n_1+l_2}\right\rangle+\left|\Phi_{21}\psi_L^{n_1+m_2}\right\rangle$). The rotation angles θ_R and θ_L of annular intensity profiles are related to the azimuth angles $\Phi_R=\Phi_{11}+\Phi_{22}$ and $\Phi_L=\Phi_{12}+\Phi_{21}$

microscope images of the fabricated chiral metasurface, respectively. The experimental setup for generating HDPBs through alignment of two cascaded metasurfaces is illustrated in Supplementary Note 5. Endowed with topological charges of $l_1=7$, $m_1=-5$, $n_1=7$, $l_2=8$, $m_2=1$ and $n_2=4$ ($l_1=7$, $m_1=4$, $n_1=-5$, $l_2=8$, $m_2=6$ and $n_2=8$), the generated HDPBs with independent polarization orders P_R and P_L of 8 and 7/2 (3/2 and 7) demonstrates 16 and 7 (3 and 14) bright lobes through RCP and LCP analyzers, as shown

in the left (right) part of Fig. 3(d). Besides, due to the axicon and Fourier lens phase modulation provided by meta_2, HDPBs possess almost identical radiuses, exhibiting perfect characteristics. In this regard, the outline of the HDPBs could also be adjustable according to the designed ellipticities γ (defined as the ratio of horizontal and vertical radiuses). Figure 3(e) shows the intensity profiles of the perfect HDPBs with ellipticities of 0.6, 0.8, 1.0 and 1.2 (with topological charges of $l_1=7$, $m_1=7$, $n_1=7$, $l_2=8$, $m_2=8$ and $n_2=8$). The normalized intensities along horizontal and vertical directions indicated by white solid and dashed lines are plotted in Fig. S4. The corresponding ellipticities are measured to be 0.62, 0.77, 0.99 and 1.24, which match well with the theoretical values and demonstrate the capability of shaping the outlines of perfect HDPBs (Supplementary Note 6). By the way, the alignment accuracy of two cascaded metasurfaces is required to be about 5 μm (see Supplementary Note 7), which can be well accessible in experiments.

In addition, the states of HDPBs on the equators of high-dimensional Poincaré spheres shown in Fig. 3(f), which are represented by azimuth angles $\Phi_R=\Phi_{11}+\Phi_{22}$ and $\Phi_L=\Phi_{12}+\Phi_{21}$ and reflect in the rotation angles θ_L and θ_R of bright lobes, is accessible to be manipulated by adjusting Φ_{12}, Φ_{11}, Φ_{22} and Φ_{21}. It is worth noting that the influence of Gouy phase on azimuth angles should be taken into careful consideration (see Supplementary Note 8 for detailed analysis). The rotation angles θ_L and θ_R of bright lobes (indicated by the white dashed lines in Fig. 3(f)), which are defined as the minimum positive angle between the center of bright lobes and the x-coordinate axis, can be employed to retrieve the azimuth angles Φ_R and Φ_L of HDPBs (see details in Supplementary equations S9e-f and Supplementary Note 9). As depicted in the four corners of Fig. 3(f), the HDPBs with different azimuth angles Φ_R and Φ_L (with $l_1=7$, m_1=-8, n_1=-9, $l_2=8$, m_2=-7 and n_2=-8), which can be expressed as $|\psi_R^{15}\rangle+|^{\Phi_{21}}\psi_L^{0}\rangle+|^{\Phi_{11}}\psi_L^{0}\rangle+\left|^{\Phi_{11}+\Phi_{22}}\psi_R^{-16}\right\rangle$ and $|\psi_L^{15}\rangle+\left|^{\Phi_{22}}\psi_R^{-1}\right\rangle+\left|^{\Phi_{12}}\psi_R^{-1}\right\rangle+\left|^{\Phi_{12}+\Phi_{21}}\psi_L^{-16}\right\rangle$, are characterized by RCP and LCP analyzers. For both RCP and LCP incidences, the generated beams via four sets of cascaded metasurfaces all present 31 bright lobes determined by polarization orders P_R and P_L of 31/2 but with different rotation angles θ_R and θ_L, corresponding to the states marked by Greek numerals I, II, III and IV featured with azimuth angles Φ_R of 270°, 0°, 90°, 180° and Φ_L of 0°, 90°, 180°, 270°. Therefore, flexible and independent manipulation of polarization orders P_L and P_R, ellipticities γ along with azimuth angles Φ_R and Φ_L of perfect HDPBs have been demonstrated in virtue of two cascaded multi-channel chiral metasurfaces.

Optical encryption based on cascaded metasurfaces

After investigating the manipulation capability of both the outline and states of HDPBs via cascaded metasurfaces, five explored independent parameters, namely γ, Φ_R, Φ_L, P_R and P_L, can be employed for optical information encoding. Furthermore, in order to construct an optical encryption system on the basis of HDPBs, two arrayed metasurfaces are implemented to enable a high-security platform with enlarged encoding capacity, as presented in Fig. 4(a). The first arrayed metasurfaces (denoted as arrayed meta_1) is composed of 16×10 meta_1 cells for generating multi-channel HyOPBs as incidences for the second arrayed metasurfaces (denoted

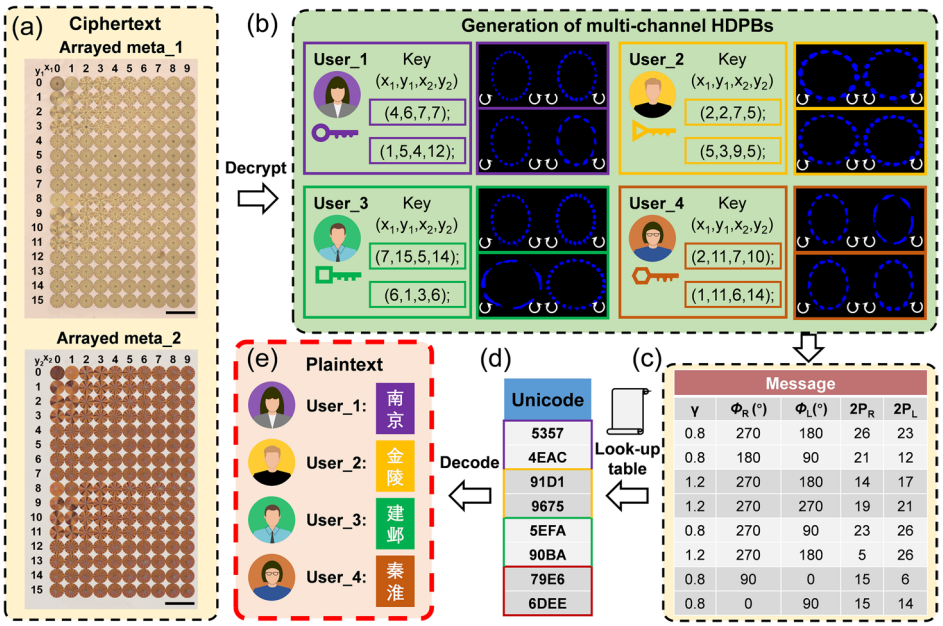

Fig. 4 Optical encryption demonstration based on cascaded metasurfaces. **a** The optical microscope images of two arrayed metasurfaces both including 16 × 10 cells which serve as ciphertext. Scale bar: 200 μm. **b** Information decryption by generating HDPBs through alignment of two metasurfaces according to the customized keys in the form of coordinates (x_1, y_1, x_2, y_2) for four users (each user possesses two keys). **c** The obtained messages about five parameters of the generated HDPBs and (**d**) the corresponding retrieved 4-bit Unicode characters based on look-up table. **e** The decrypted plaintext of four Chinese characters through Unicode encoding by four users

as arrayed meta_2) consisting of 16 × 10 meta_2 cells (see Tables S2 and S3 in Supplementary Note 10). Through combination of different cells in two arrayed metasurfaces, an abundant number of perfect HDPBs featured with different parameters are available. As a demonstration, the plaintext messages of four Chinese words "南京", "金陵", "建邺" and "秦淮" (four names of Nanjing in Chinese), are encrypted into two metasurfaces (ciphertext) through the Unicode encoding in the form of five parameters of perfect HDPBs, accompanied with the customized keys in the form of coordinates (x_1, y_1, x_2, y_2). Once the ciphertext and customized keys are transferred into four users, the decryption process begins with the alignment of two arrayed metasurfaces. In accordance with the received coordinates (x_1, y_1, x_2, y_2), the target cells are subsequently illuminated by 470 nm RCP and LCP light for generation of perfect HDPBs, respectively. As a consequence, each user who owns two keys could obtain two sets of HDPBs, depicted in Fig. 4(b). Then, the parameters of HDPBs, including γ, Φ_R and Φ_L, P_R and P_L, are retrieved and transformed into digital forms, as listed in Fig. 4(c). With reference to the self-defined look-up table in Supplementary Note 11 each user could translate the obtained messages into two four-bit hexadecimal digits in Fig. 4(d). As indicated in Fig. 4(e), the ciphertext would eventually be decoded through Unicode encoding as "南京", "金陵", "建邺" and "秦淮", respectively. So far, the optical encryption platform has been established via two cascaded metasurfaces based on multi-channel perfect HDPBs.

Discussion and conclusion

Compared with other optical encryption schemes based on metasurface [21, 26, 30, 31, 45], the proposed optical encryption platform utilizes the combination of two arrayed metasurfaces as keys to achieve an enlarged key space. Meanwhile, the encoding space has been greatly expanded to be adaptive with Unicode encoding thanks to sufficient DoFs carried by HDPBs and multi-channel light field manipulation provided by chiral metasurfaces (see Supplementary Note 12 for evaluation of key and encoding spaces). It should be emphasized that, benefiting from the compactness of metasurface and extended DoFs of HDPBs, the arrayed metasurfaces could easily be scaled up to establish larger key and encoding spaces for high-capacity optical information encryption with unprecedented level of security.

To conclude, we have proposed and experimentally demonstrated perfect HDPBs for optical encryption with large capacity and high security through cascaded metasurfaces. Attributed to the spin-decoupled wavefront tailoring capability of chiral meta-atoms, a single-layer metasurface is applied to function as the combination of quarter wave plate, spiral phase plate, axicon and Fourier lens to produce multi-channel perfect HyOPBs by linear superposition of transmitted co-polarized and cross-polarized perfect vortex beams. By introducing another chiral metasurface to generate HyOPBs as the second-level input beam, multi-channel HDPBs are constructed under RCP and LCP incidences through two cascaded metasurface. Particularly, five parameters of perfect HDPBs, including ellipticities, polarization orders and azimuth angles for RCP and LCP incidences, can be independently manipulated at will for optical information encoding. By virtue of two cascaded metasurfaces containing 16×10 cells, an optical encryption scheme with enhanced encoding capacity and security level has been constructed by encrypting information into perfect HDPBs which can only be obtained through alignment of specific cells in two arrayed metasurfaces. Overall, this work for optical information encryption and encoding via multi-channel perfect HDPBs may promote the development of miniaturization and integration of optical encryption system with high security and inspire intriguing applications of Poincaré beams for high-capacity optical communications and quantum information.

Methods

Numerical simulations

Numerical simulations were performed to investigate the phase shifts of both co-polarized and cross-polarized channels of chiral meta-atoms through finite-difference time domain (FDTD) methods. The refractive index of SiN_x used in simulations was $n = 2.032 + 0.0013i$, which was obtained from experimental samples measured by spectroscopic ellipsometer. A 470 nm plane-wave source was employed to illuminate chiral meta-atoms from substrate. Perfectly matched layer (PML) was utilized as boundary condition along the propagation direction of light source while periodic boundary conditions are applied along all the in-plane directions.

Device fabrication

The samples were prepared on a fused silica substrate through deposition of SiN_x layer with 1.2 μm height using plasma-enhanced chemical vapor deposition (PECVD).

Then, an electron beam resist (PMMA-A4) with the thickness of 200 nm was spin-coated on top of the SiN_x layer. The patterns of chiral meta-atoms were subsequently defined on PMMA resist by Electron-beam lithography (EBL) system (ELS-F125, Elionix). After development, the generated pattern was transferring to an electron beam evaporated chromium layer, which served as a hard mask for the following dry etching process of SiN_x layer in a mixture of CHF_3 and SF_6 plasma (Oxford Instruments, PlasmaPro100 Cobra300). At last, the remaining chromium mask was removed by a solution of ammonium cerium nitrate.

Optical characterization

A 470 nm laser was utilized for optical measurement and focused onto the fabricated metasurfaces through an objective (20×, NA = 0.40). The polarization states of the incident light were controlled by the combination of linear polarizer and quarter-wave plate. After illuminating the metasurface/cascaded metasurface, the transmitted light was subsequently collected by an objective (20×, NA = 0.40) and analyzed by polarizers. Subsequently, the intensity profiles of the generated Poincaré beams were recorded using a CMOS camera. The alignment of two cascaded metasurfaces is detailed in Supplementary Note 5.

Abbreviations

DOFs	Degrees of freedom
HDPBs	High-dimensional Poincaré beams
OAM	Orbital angular momentum
HyOPBs	Hybrid-order Poincaré beams
RCP	Right-handed circular polarized
LCP	Left-handed circular polarized
H-polarized	Horizontal linearly polarized
V-polarized	Vertical linearly polarized
FDTD	Finite-difference time domain
PML	Perfectly matched layer
PECVD	Plasma-enhanced chemical vapor deposition
EBL	Electron-beam lithography

Supplementary Information

The online version contains supplementary material available at https://doi.org/10.1186/s43074-024-00125-8.

Supplementary Material 1.

Acknowledgements
Not applicable.

Authors' contributions
C.C., J.J. and T.L. conceived the concept. C.C. and J.J. proposed the metasurface design and performed the numerical simulations; J.S. and J.L. fabricated the samples with the help of C.H. and K.Q.; J.J. and C.C. performed the optical measurements with the help of X.Y. and J.W.; J.J., C.C., Z.W., W.S., T.L. and S.Z. discussed the results; J.J., and C.C. wrote the manuscript with the help of Z.W. and W.S.; T.L. supervised the project.

Funding
The authors acknowledge the funding provided by National Key Research and Development Program of China (2022YFA1404301), National Natural Science Foundation of China (Nos. 62325504, 62305149, 92250304, 62288101), and Dengfeng Project B of Nanjing University. The authors acknowledge the micro-fabrication center of the National Laboratory of Solid State Microstructures (NLSSM) for technique support.

Availability of data and materials
The source data are available from the corresponding author upon reasonable request. All data needed to evaluate the conclusion are present in the manuscript and/or the Supplementary Information.

Declarations

Ethics approval and consent to participate
Not applicable.

Consent for publication
All authors agreed to publish this paper.

Competing interests
The authors declare no conflicts of interest.

Received: 17 January 2024 Revised: 6 March 2024 Accepted: 11 March 2024
Published online: 17 April 2024

References

1. Matoba O, Nomura T, Perez-Cabre E, Millan MS, Javidi B. Optical techniques for information security. Proc IEEE. 2009;97(6):1128–48.
2. Chen W, Javidi B, Chen X. Advances in optical security systems. Adv Opt Photonics. 2014;6(2):120–55.
3. Liu S, Guo C, Sheridan JT. A review of optical image encryption techniques. Opt Laser Technol. 2014;57:327–42.
4. Jiao S, Zhou C, Shi Y, Zou W, Li X. Review on optical image hiding and watermarking techniques. Opt Laser Technol. 2019;109:370–80.
5. Liu S, Liu X, Yuan J, Bao J. Multidimensional information encryption and storage: when the input is light. Res (Wash D C). 2021;2021:7897849.
6. Yu NF, Genevet P, Kats MA, Aieta F, Tetienne JP, Capasso F, et al. Light propagation with phase discontinuities: generalized laws of reflection and refraction. Science. 2011;334(6054):333–7.
7. Yu N, Capasso F. Flat optics with designer metasurfaces. Nat Mater. 2014;13(2):139–50.
8. Zhao R, Huang L, Wang Y. Recent advances in multi-dimensional metasurfaces holographic technologies. PhotoniX. 2020;1(1):20.
9. Deng Z-L, Wang Z-Q, Li F-J, Hu M-X, Li X. Multi-freedom metasurface empowered vectorial holography. Nanophotonics. 2022;11(9):1725–39.
10. Li T, Chen C, Xiao X, Chen J, Hu S, Zhu S. Revolutionary meta-imaging: from superlens to metalens. Photonics Insights. 2023;2(1):R01.
11. Yang H, Ou K, Wan H, Hu Y, Wei Z, Jia H, et al. Metasurface-empowered optical cryptography. Mater Today. 2023;67:424–45.
12. Jung C, Kim G, Jeong M, Jang J, Dong Z, Badloe T, et al. Metasurface-driven optically variable devices. Chem Rev. 2021;121(21):13013–50.
13. So S, Mun J, Park J, Rho J. Revisiting the design strategies for metasurfaces: fundamental physics, optimization, and beyond. Adv Mater. 2023;35(43):2206399.
14. Kamali SM, Arbabi E, Arbabi A, Horie Y, Faraji-Dana M, Faraon A. Angle-multiplexed metasurfaces: encoding independent wavefronts in a single metasurface under different illumination angles. Phys Rev X. 2017;7(4):041056.
15. Wan S, Wan C, Dai C, Li Z, Tang J, Zheng G, et al. Angular-multiplexing metasurface: building up independent-encoded amplitude/phase dictionary for angular illumination. Adv Opt Mater. 2021;9(22):2101547.
16. Wan S, Tang J, Wan C, Li Z, Li Z. Angular-encrypted quad-fold display of nanoprinting and meta-holography for optical information storage. Adv Opt Mater. 2022;10(11):2102820.
17. Lim KTP, Liu H, Liu Y, Yang JKW. Holographic colour prints for enhanced optical security by combined phase and amplitude control. Nat Commun. 2019;10(1):25.
18. Yue F, Zhang C, Zang XF, Wen D, Gerardot BD, Zhang S, et al. High-resolution grayscale image hidden in a laser beam. Light Sci Appl. 2018;7:17129.
19. Yang H, Jiang Y, Hu Y, Ou K, Duan H. Noninterleaved metasurface for full-polarization three-dimensional vectorial holography. Laser Photonics Rev. 2022;16(11):2200351.
20. Zhou H, Sain B, Wang Y, Schlickriede C, Zhao R, Zhang X, et al. Polarization-encrypted orbital angular momentum multiplexed metasurface holography. ACS Nano. 2020;14(5):5553–9.
21. Ren H, Fang X, Jang J, Burger J, Rho J, Maier SA. Complex-amplitude metasurface-based orbital angular momentum holography in momentum space. Nat Nanotechnol. 2020;15(11):948–55.
22. Jin L, Huang Y-W, Jin Z, Devlin RC, Dong Z, Mei S, et al. Dielectric multi-momentum meta-transformer in the visible. Nat Commun. 2019;10(1):4789.
23. Ren H, Briere G, Fang X, Ni P, Sawant R, Héron S, et al. Metasurface orbital angular momentum holography. Nat Commun. 2019;10(1):2986.
24. Qu G, Yang W, Song Q, Liu Y, Qiu CW, Han J, et al. Reprogrammable meta-hologram for optical encryption. Nat Commun. 2020;11(1):5484.
25. Georgi P, Wei QS, Sain B, Schlickriede C, Wang YT, Huang LL, et al. Optical secret sharing with cascaded metasurface holography. Sci Adv. 2021;7(16):eabf9718.
26. Luo X, Hu Y, Li X, Jiang Y, Wang Y, Dai P, et al. Integrated metasurfaces with microprints and helicity-multiplexed holograms for real-time optical encryption. Adv Opt Mater. 2020;8(8):1902020.
27. Kim J, Jeon D, Seong J, Badloe T, Jeon N, Kim G, et al. Photonic encryption platform via dual-band vectorial metaholograms in the ultraviolet and visible. ACS Nano. 2022;16(3):3546–53.
28. Guo X, Zhong J, Li B, Qi S, Li Y, Li P, et al. Full-color holographic display and encryption with full-polarization degree of freedom. Adv Mater. 2022;34(3):e2103192.

29. Li J, Guan Z, Liu HC, He Z, Li Z, Yu S, et al. Metasurface-assisted indirect-observation cryptographic system. Laser Photonics Rev. 2022;17(1):2200342.
30. Yang H, He P, Ou K, Hu Y, Jiang Y, Ou X, et al. Angular momentum holography via a minimalist metasurface for optical nested encryption. Light Sci Appl. 2023;12(1):79.
31. Jin L, Dong Z, Mei S, Yu YF, Wei Z, Pan Z, et al. Noninterleaved Metasurface for (2(6)-1) Spin- and Wavelength-Encoded Holograms. Nano Lett. 2018;18(12):8016–24.
32. Bao Y, Yu Y, Xu H, Lin Q, Wang Y, Li J, et al. Coherent pixel design of metasurfaces for multidimensional optical control of multiple printing-image switching and encoding. Adv Funct Mater. 2018;28(51):1805306.
33 Zheng PX, Dai Q, Li ZL, Ye ZY, Xiong J, Liu HC, et al. Metasurface-based key for computational imaging encryption. Sci Adv. 2021;7(21):eabg0363.
34. Guo X, Li P, Zhong J, Wen D, Wei B, Liu S, et al. Stokes meta-hologram toward optical cryptography. Nat Commun. 2022;13(1):6687.
35. Kim I, Jang J, Kim G, Lee J, Badloe T, Mun J, et al. Pixelated bifunctional metasurface-driven dynamic vectorial holographic color prints for photonic security platform. Nat Commun. 2021;12(1):3614.
36. Xiong B, Xu Y, Wang J, Li L, Deng L, Cheng F, et al. Realizing colorful holographic mimicry by metasurfaces. Adv Mater. 2021;33(21):e2005864.
37. Hu Y, Ou X, Zeng T, Lai J, Zhang J, Li X, et al. Electrically tunable multifunctional polarization-dependent metasurfaces integrated with liquid crystals in the visible Region. Nano Lett. 2021;21(11):4554–62.
38. Gao H, Fan X, Xiong W, Hong M. Recent advances in optical dynamic meta-holography. Opto-Electronic Adv. 2021;4(11):210030.
39. Yi X, Liu Y, Ling X, Zhou X, Ke Y, Luo H, et al. Hybrid-order Poincaré sphere. Phys Rev A. 2015;91(2):023801.
40. Rosales-Guzmán C, Ndagano B, Forbes A. A review of complex vector light fields and their applications. J Opt. 2018;20(12):123001.
41. Bao Y, Ni J, Qiu CW. A minimalist single-layer metasurface for arbitrary and full control of vector vortex beams. Adv Mater. 2020;32(6):e1905659.
42. Jiang ZH, Kang L, Yue T, Xu HX, Yang Y, Jin Z, et al. A Single noninterleaved metasurface for high-capacity and flexible mode multiplexing of higher-order poincare sphere beams. Adv Mater. 2020;32(6):e1903983.
43. Chen Y, Xia KY, Shen WG, Gao J, Yan ZQ, Jiao ZQ, et al. Vector vortex beam emitter embedded in a photonic chip. Phys Rev Lett. 2020;124(15):153601.
44. Yang Y, Ren Y-X, Chen M, Arita Y, Rosales-Guzmán C. Optical trapping with structured light: a review. Adv Photonics. 2021;3(03):034001.
45. Liu M, Huo P, Zhu W, Zhang C, Zhang S, Song M, et al. Broadband generation of perfect Poincare beams via dielectric spin-multiplexed metasurface. Nat Commun. 2021;12(1):2230.
46. Dong Z, Chen Y, Wang F, Cai Y, Friberg AT, Setälä T. Encoding higher-order polarization states into robust partially coherent optical beams. Phy Rev Appl. 2022;18(3):034036.
47. Deng L, Jin R, Xu Y, Liu Y. Structured light generation using angle-multiplexed metasurfaces. Adv Opt Mater. 2023;11(16):2300299.
48. Li H, Zheng C, Liu J, Xu H, Song C, Yang F, et al. Binary encoding-inspired generation of vector vortex beams. Sci China Phys Mech Astron. 2023;66(5):254212.
49. Wang S, Wen S, Deng ZL, Li X, Yang Y. Metasurface-based solid poincare sphere polarizer. Phys Rev Lett. 2023;130(12):123801.
50. Jang J, Badloe T, Rho J. Unlocking the future of optical security with metasurfaces. Light Sci Appl. 2021;10(1):144.
51. Cai X, Tang R, Zhou H, Li Q, Ma S, Wang D, et al. Dynamically controlling terahertz wavefronts with cascaded metasurfaces. Adv Photonics. 2021;3(03):036003.
52. Mei F, Qu G, Sha X, Han J, Yu M, Li H, et al. Cascaded metasurfaces for high-purity vortex generation. Nat Commun. 2023;14(1):6410.
53. Chen C, Gao SL, Song WG, Li HM, Zhu SN, Li T. Metasurfaces with planar chiral meta-atoms for spin light manipulation. Nano Lett. 2021;21(4):1815–21.
54. Chen C, Ye X, Sun JC, Chen YX, Huang CY, Xiao XJ, et al. Bifacial-metasurface-enabled pancake metalens with polarized space folding. Optica. 2022;9(12):1314–22.

Publisher's Note